frontiers | Frontiers in Earth Science

TYPE Original Research
PUBLISHED 12 July 2024
DOI 10.3389/feart.2024.1401624

Coupling noble gas and alkane gas isotopes to constrain normally pressured shale gas expulsion in SE Sichuan Basin, China

Jiaxin Li[1,2], Yunhai Wang[2], Dazhi Fang[2], Zhigang Wen[1] and Chenjun Wu[1]*

[1]Hubei Key Laboratory of Petroleum Geochemistry and Environment, Yangtze University, Wuhan, China, [2]Sinopec East China Oil and Gas Company, Nanjing, China

Check for updates

OPEN ACCESS

EDITED BY
Wenguang Wang,
Northeast Petroleum University, China

REVIEWED BY
Mianmo Meng,
China University of Geosciences Wuhan, China
Chao Li,
Northwest Institute of Eco-Environment and Resources (CAS), China

*CORRESPONDENCE
Chenjun Wu,
chenjun.wu@yangtzeu.edu.cn

RECEIVED 15 March 2024
ACCEPTED 10 June 2024
PUBLISHED 12 July 2024

CITATION
Li J, Wang Y, Fang D, Wen Z and Wu C (2024), Coupling noble gas and alkane gas isotopes to constrain normally pressured shale gas expulsion in SE Sichuan Basin, China.
Front. Earth Sci. 12:1401624.
doi: 10.3389/feart.2024.1401624

The molecular and isotopic compositions of shale gases exhibit substantial differences under different storage conditions. Gas geochemistry is widely used when evaluating gas accumulation and expulsion in petroleum systems. Gas geochemical characteristics can provide important references for determining the enrichment mechanism of shale gas reservoirs and predicting shale gas production capacity in different regions. In tectonically stable regions with similar reservoir formation and evolution histories, shale gas reservoirs are expected to exhibit favorable storage conditions with only relatively small variations in gas geochemical characteristics. In tectonically active regions, shale gas preservation conditions are expected to be more variable. In this study, we systematically analyzed the stable isotope signatures ($\delta^{13}C$ and δD) of alkane gases (CH_4, C_2H_6, and C_3H_8), along with noble gas compositions and isotopic signatures, of normally pressured Wufeng-Longmaxi marine shale gas samples comprising a continuous pressure coefficient series from a structurally active region at the transition between an orogenic belt and the southeastern (SE) Sichuan Basin, China. The relationships between noble gas contents, isotopic signatures, and shale gas yields were evaluated, and a mechanism for normally pressured shale gas accumulation and expulsion was presented. The $\delta^{13}C$ and δD data suggest that the normally pressured shale gas originated from late-mature thermogenic generation, equivalent to shale gas from other production areas in the inner Sichuan Basin. Gas dryness ratios $[C_1/(C_2 + C_3)]$ exhibit negative relationships with $\delta^{13}C_1$ and $\delta^{13}C_2$. Normally pressured shale gas yields exhibit a negative correlation with $\delta^{13}C$ and a positive correlation with $[C_1/(C_2 + C_3)]$, suggesting differences in shale gas accumulation and expulsion across the studied region related to changes in the pressure coefficient. Noble gas isotope data suggest that the normally pressured Longmaxi shale gas received a substantial contribution of crust-derived He. Coupling noble gas and stable C/H isotope data reveals that the abundance of He and Ar, along with the $\delta^{13}C$ signatures of alkane gases, is affected by the abundance of shale gas during the accumulation and expulsion process. The noble gas and stable isotope distribution trends presented herein can be used to evaluate Wufeng-Longmaxi's normally pressured shale gas accumulation and expulsion in complex structural areas of the southeastern Sichuan Basin. Better preservation conditions accompanying lower tectonic activity will normally result in higher shale gas production and a lower concentration of noble gases. The above findings show that gas geochemical characteristics could be used as effective evaluation indicators for determining shale gas accumulation mechanisms in tectonically active regions.

KEYWORDS

normally pressured shale gas, noble gas, carbon isotope, accumulation, expulsion

1 Introduction

Gas geochemical characteristics are important tools for studying the formation mechanism of natural gas reservoirs. The fractionation of alkane gas carbon isotopes in natural gas, owing to mass transport, is widely used to identify genetic types of natural gas, as well as oil and gas source correlation and alteration processes (Schoell, 1988; Whiticar, 1996; Xia and Tang, 2012). Owing to chemical inertness, noble gases are not impacted by secondary chemical processes, no matter whether the chemical reactions are inorganic or organic (Ozima and Podosek, 2017; Byrne et al., 2018). Noble gas isotope data have been widely used as important gas tracers for a variety of subsurface fluid transport processes in petroleum systems (Zhou et al., 2012; Burnard et al., 2013; Wang et al., 2013; Byrne et al., 2017; Byrne et al., 2020; Zhang et al., 2019).

Shale gas is considered a notable discovery in terms of natural gas exploration in the Sichuan Basin, given its great resource potential (Dai et al., 2014; Zou et al., 2015; Dong et al., 2016). Multiple exploration breakthroughs have been achieved in the Sichuan Basin, with the discovery of several very large shale gas fields, including Fuling, Weiyuan, Weirong, and Zhaotong (Jiang et al., 2020; Ma et al., 2020; Qiu et al., 2020; Zhao et al., 2020; Zou et al., 2021). The aforementioned successful shale gas fields have all targeted deep and high/over-pressured shale layers at depths >2000 m and pressure coefficients >1.3. In contrast, orogenic processes have caused Wufeng-Longmaxi shale to be markedly uplifted in Sichuan Basin–margin transitional regions. Hence, shale layers in the southeastern (SE) Sichuan Basin are now characterized by low burial depths (<2000 m) and low pressure coefficients (<1.3), leading to the formation of normally pressured shale gas.

Shale gas exploration in the United States began in normally pressured organic-rich shale layers (Guo et al., 2015; Hu et al., 2015). Before 2004, the main shale gas fields, such as the Marcellus shale gas field in the Appalachian Basin and Ohio shale gas field, were dominated by normally pressured shale gas, characterized by low-pressure or normal-pressure conditions (Lancaster et al., 1989; Curtis, 2002; Montgomery et al., 2006; Pollastro et al., 2007; Darabi et al., 2012; Meng et al., 2023). The typical characteristics of normally pressured shale gas in the United States are a continuous distribution of organic-rich shales, low thermal evolution, and a stable tectonic environment (Guo, 2016, Guo et al., 2020; Jiang et al., 2022). The thermal maturity of normally pressured shale gas in the United States is normally <1.5%, with an adsorbed shale gas content >50%. In contrast to low-maturity normally pressured shale gas in the United States, normally pressured shale gas exploration in China has achieved notable success in highly mature shales (Guo et al., 2020). Normally pressured organic-rich shale layers are widely distributed along the margins of the Sichuan Basin. Currently, the Nanchuan–Wulong regions, located in the southeastern Sichuan Basin, are the only successfully developed normally pressured shale gas fields in this basin. Compared with high-/over-pressured shale gas reservoirs, normally pressured shale gas reservoirs have the characteristics of weak formation energy, complex ground stress fields, low single-well production, high drilling and production costs, a wide distribution area, a large total resource, and low resource abundance (Guo et al., 2020; He, 2021). Under existing technical and economic conditions, commercial development of normally pressured shale gas faces considerable challenges. Previous studies have revealed tectonic deformation, such as folding, to be the key factor in controlling the quality of Wufeng-Longmaxi shale gas preservation conditions. More intense strain results in more free gas migrating to pressure-relief areas, such as eroded areas, permeable faults, and fracture zones. Meanwhile, owing to pressure reduction and desorption, the adsorbed gas will be converted into free gas and also dissipate, resulting in the further reduction of shale gas content or potentially no gas at all. Therefore, the intensity of the tectonic strain controls the quality of preservation conditions, affecting the gas content of shale and the proportion of free gas, and determines the enrichment of shale gas reservoirs (He et al., 2019; He, 2021).

Geological studies suggest that multi-stage tectonic movement has occurred in the southeastern Sichuan Basin, causing shale gas preservation conditions to be degraded (He et al., 2019). Gas geochemistry has been widely used to provide important information in the evaluation of shale gas type, origin, evolution, migration, and accumulation (Dai et al., 2014; Cao et al., 2018; Cao et al., 2020; Chen et al., 2020; Liu et al., 2021; Wang et al., 2022). Wang et al. (2022) studied the chemical compositions and isotopic signatures of alkane gases, He, and Ar associated with Lower Paleozoic shale gas in the southern Sichuan Basin. Cao et al. (2020) analyzed shale gas origin and evolution using the stable carbon isotope signature ($\delta^{13}C$) of alkane gases and the geochemistry of noble gases. Liu et al. (2021) used noble gas and C/H isotopic analyses to evaluate reservoir compartmentalization in the Wufeng-Longmaxi organic-rich shale and determined the geologic causation mechanism (e.g., tectonic activity). Most of the aforementioned research has focused on well-developed high-/over-pressured shale reservoirs; however, the accumulation and expulsion mechanisms of normally pressured shale gas reservoirs have received much less attention.

In this study, normally pressured shale gas samples from various structural positions across the southeastern Sichuan Basin were collected, and their alkane gas (methane (CH_4), ethane (C_2H_6), and propane (C_3H_8)) stable isotope ($\delta^{13}C$ and δD) and noble gas isotope signatures were analyzed. The main objectives of this study were to 1) reveal the coupling relationship between hydrocarbon gas isotope signatures and shale gas yield; 2) understand the origin of noble gas from normally pressured shale gas reservoirs; 3) determine the accumulation and expulsion mechanisms of normally pressured shale gas in the tectonically complex margin of the southeastern Sichuan Basin; and 4) provide insights into the enrichment mechanism of shale gas reservoirs and the prediction of shale gas production capacity in other structurally complex regions of the world.

2 Geological setting

The Sichuan Basin is located in southwest China, northwest of the Yangtze metaplatform; tectonically, it is an important gas-producing sedimentary basin in China. Wufeng–Longmaxi organic-rich shales are widely distributed across the Sichuan Basin and surrounding regions and are key exploration and evaluation targets for shale gas reservoirs (Dai et al., 2014; Gao et al., 2014; Zhao et al., 2019). Our study area is located in the southeastern Sichuan Basin and comprises a basin-margin transition belt and an extra-basin complex fold belt (Figure 1).

The basin-margin transition belt is located between the Sichuan Basin and a complex fold belt lying exterior to the basin; it shows a higher level of tectonic deformation compared with most parts of the Sichuan Basin, but deformation is weaker than that outside of the basin. The region has experienced multiple tectonic phases, including during the Caledonian, Hercynian, Indosinian, and Yanshan–Himalayan periods, with the latter having the strongest impact. This has laid the foundation for the current structural pattern, dominated by northeast–southwest-trending synclines and anticlines. From east to west, the basin-margin transition belt includes seven tectonic units: Shimen slope, Shiqiao fault depression, Pingqiao anticline, Yuanjiagou syncline, Dongsheng anticline, Shentongba syncline, and Yangchungou anticline. Wufeng–Longmaxi organic-rich shales in this basin-margin transition belt are buried under high- to normal-pressure conditions, with pressure coefficients ranging between 1.10 and 1.35.

The extra-basin complex fold belt exhibits an increased degree of uplift-related erosion, with the Longmaxi Formation being almost completely denuded in anticlinal regions. Hence, Longmaxi organic-rich shales mainly occur in residual synclines, such as the Wulong, Sangzeping, and Daozhen synclines. The present burial depth of Longmaxi organic-rich shales in these residual synclines ranges from 1,000 to 3,500 m (He et al., 2019), where they are buried under typical normal-pressure conditions with pressure coefficients ranging from 0.95 to 1.10.

3 Sampling and analytical methodology

3.1 Shale gas samples

Eighteen shale gas samples from the southeastern Sichuan Basin were collected using steel cylinder gas containers with a maximum gas pressure capacity of 15 MPa and a maximum volume of 1,000 mL. To avoid atmospheric contamination, the containers were flushed with wellhead gas at least 10 times before gas collection. The studied shale gas samples were collected from the sweet shale gas layer (Wufeng–Longmaxi Formation) based on a continuous pressure coefficient series moving from the intra-basin and basin-margin transition belt toward the basin exterior; specifically, they were collected from Pingqiao (PQ), Dongsheng (DS), Jinfo (JF), Wulong (WL), and Pengshui (PS). The pressure coefficients for the Long-1 shale gas from these regions were 1.35 (PQ), 1.20–1.35 (DS), 1.12–1.20 (JF), 1.08 (WL), and 0.98 (PS), respectively.

3.2 Analytical methodology

The chemical compositions of non-hydrocarbon gases (CO_2, H_2, H_2S, N_2, and He) and hydrocarbon gases were examined. Non-hydrocarbon molecular compositions were analyzed using a gas composition mass spectrometer (MAT-271). Hydrocarbon gas compositions were analyzed using a gas chromatograph (GC, Agilent 6890N) equipped with an FID detector. To differentiate each of the individual hydrocarbon gas components (e.g., CH_4, C_2H_6, and C_3H_8), an aluminum oxide capillary column with a length of 50 m and a diameter of 0.53 mm was used. The oven temperature setting for GC analysis was set at 30°C for 10 min, followed by an increase to a target temperature of 180°C at a heating rate of 10°C/min, and then maintained at the target temperature for 20–30 min.

An Agilent 6890N GC equipped with an isotope ratio mass spectrometer (IRMS, Delta plus XP) was used to determine the $\delta^{13}C$ signatures of individual hydrocarbon gas components. The operating temperature for $\delta^{13}C$ analysis was set at 30°C for 3 min, followed by an increase to a target temperature of 250°C at a heating rate of 10°C/min, and then maintained at the target temperature for 50 min. To calculate the $\delta^{13}C$ values of hydrocarbon gases, three pulses of standard pure CO_2 gas were injected into the GC–IRMS instrument. The overall analytical precision was ±3‰.

A MAT-253 IRMS coupled with an HP6890 GC instrument was used to analyze shale gas H isotopes. CH_4 and C_2H_6 components were chromatographically distinguished using a fused silica capillary column (HP-PLOT Q, 30 m × 0.32 mm × 20 μm). The operating GC temperature for H isotope analysis was set at 40°C for 5 min, followed by an increase to 80°C at a heating rate of 5°C/min, a further increase to 140°C at a heating rate of 10°C/min, and a final increase to a target temperature of 260°C at a heating rate of 30°C/min (Xing et al., 2021). The pyrolysis-oven temperature was set at 1,450°C, and a standard H_2 sample was used as the reference gas. The accuracy of the H isotope analysis was approximately ±3‰. Hydrogen isotope data are reported in δ notation (δD, ‰) relative to Vienna Standard Mean Ocean Water (VSMOW = 0.0‰). An internal standard was measured to calibrate the δD data for the studied shale gas samples (Cao et al., 2020).

Abundances and isotopic compositions of noble gases (He, Ne, and Ar) were measured using a noble gas isotope mass spectrometer (Noblesse SFT). The shale gas sample container was first connected to the purification vacuum system. After the system reached vacuum, the gas sample was introduced into a gas pipette with a volume of 8.5 cm^3. According to the pressure and temperature variations in the gas pipette before and after the gas

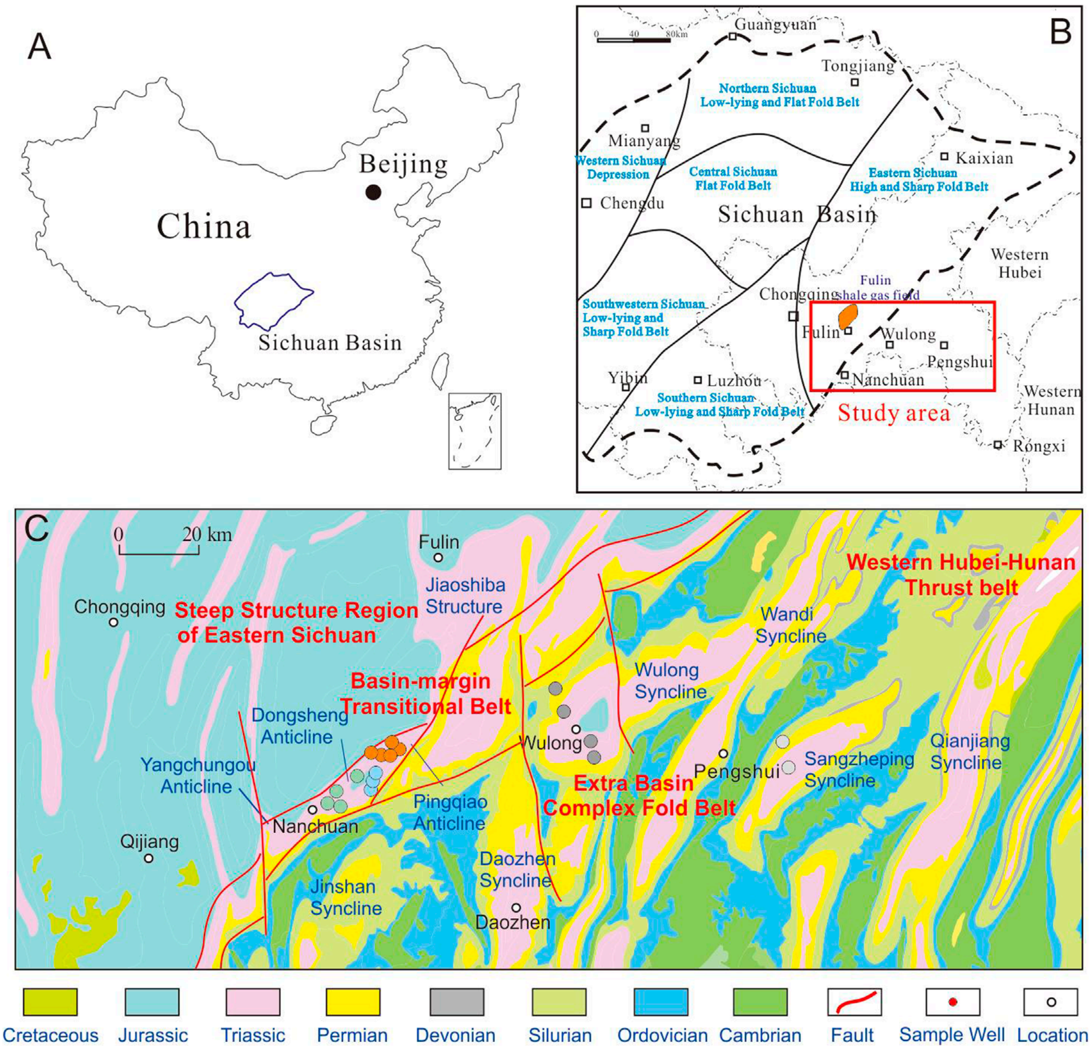

FIGURE 1
Location and degree of geologic deformation of the study area in the southeastern Sichuan Basin.

sample introduction, the absolute amount of gas sample introduced was calculated. Then, 1.5 cm^3 of the gas sample was further introduced to the online noble gas isotope mass spectrometer for noble gas purification. Details of the analytical procedure for noble gas abundance and isotope composition determination can be found in Cao et al. (2018).

4 Results

4.1 Shale gas yields

Shale gas yields from the basin-margin transition belt and extra-basin complex fold belt vary markedly. Considering that drilling wells in different structural zones are currently in different stages of production, daily shale gas production values for the first 500 production days were compared herein (Table 1; Figure 2). Compared with the highly pressured Jiaoshiba shale gas production region (e.g., 20.3 × 10^4 m^3/day for well JY1), daily shale gas production values in the study area were much lower. Shale gas production in the PQ area was the highest, ranging from 4.19 × 10^4 to 6.55 × 10^4 m^3/day (average: 5.55 × 10^4 m^3/day). The average daily shale gas production values for the DS and JF areas were 3.32 × 10^4 and 3.40 × 10^4 m^3/day, respectively. Shale gas production in the extra-basin complex fold belt was much lower, with average values of 2.15 × 10^4 m^3/day for the WL area and 0.77 × 10^4 m^3/day for the PS area. In general, daily shale gas production exhibited a decreasing trend with a decreasing pressure coefficient across the study area.

4.2 Major gas compositions

Shale gas compositions from 18 wells within the Wufeng-Longmaxi Formation in the southeastern Sichuan Basin are shown in Table 1. All samples were dominated by CH_4, with

 10.3389/feart.2024.1401624

TABLE 1 Chemical and carbon isotope ($\delta^{13}C$) compositions of normally pressured shale gas samples in the southeastern Sichuan Basin.

Area	Well	Gas yield (m^3/d)	Gas composition (%)					$\delta^{13}C$ (‰)		$\delta^{13}D$ (‰)	
			CH_4	C_2H_6	C_3H_8	N_2	CO_2	$\delta^{13}C_1$	$\delta^{13}C_2$	$\delta^{13}DC_1$	$\delta^{13}DC_2$
PQ	JY194-A	4.19	96.47	0.28	0.01	3.11	0.05	−35.2	−37.5	−162.2	−105.4
	JY194-B	6.43	98.80	0.37	0.01	0.77	0.01	−36.5	−37.6	−163.2	−126.0
	JY194-C	5.91	98.31	0.39	0.01	0.96	0.24	−34	−37.8	−162.5	−125.1
	JY195-A	6.55	98.50	0.40	0.01	1.05	—	−32	−35.3	−165.4	−131.2
	JY197-A	4.69	98.54	0.42	0.01	0.84	0.16	−33.8	−37.5	−164.8	−121.4
JF	JY204-A	5.25	98.30	0.39	0.01	0.92	0.30	−33.6	−36.2	−160.3	−119.7
	JY204-B	3.41	98.31	0.40	0.01	0.91	0.31	−33	−36.3	−161.3	−131.2
	JY204-C	1.55	86.03	0.32	0.01	13.29	0.32	−32.7	−36.1	−160.8	−94.2
DS	SY-A	4.28	98.40	0.46	0.01	0.76	0.32	−34.4	−38	−163.8	−128.9
	SY-B	3.46	98.26	0.41	0.01	1.14	0.04	−33.9	−37	−162.8	−126.7
	SY-C	2.48	98.38	0.44	0.01	0.79	0.32	−34.3	−38.2	−163.8	−128.2
	SY-D	3.04	98.41	0.40	0.01	0.94	0.19	−32.6	−36.4	−163.4	−129.8
WL	LY-A	3.04	97.92	0.57	0.02	1.34	0.12	−30.7	−34.5	−161.1	−150.6
	LY-B	2.44	97.19	0.61	0.02	1.93	0.08	−32	−34.8	−163.7	−134.9
	PD-A	0.69	98.05	0.63	0.01	1.24	0.00	−30.6	−36.2	−158.6	−178.6
	LY-C	2.42	96.62	0.64	0.01	2.59	0.07	−29.6	−34.6	−161.4	−162.1
PS	PY-A	0.98	95.99	0.54	0.01	2.82	0.18	−30.7	−33.4	−161.9	−140.1
	PY-B	0.56	97.21	0.99	0.02	1.64	0.10	−30.9	−33.4	−163.0	−159.1

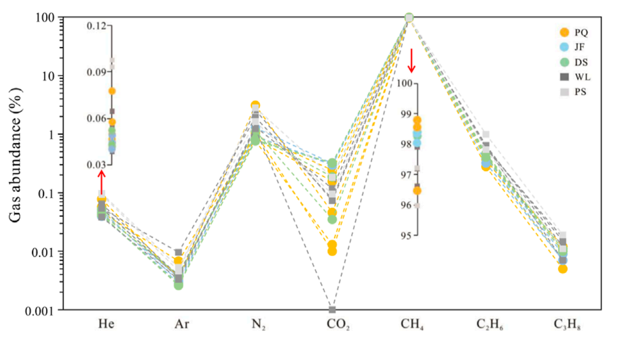

FIGURE 2
Variation in gas composition in normally pressured Longmaxi shale gas from the southeastern Sichuan Basin.

minor amounts of C_2H_6 and non-hydrocarbon gases (e.g., N_2, CO_2, and He). The CH_4 content ranged from 95.99% to 98.8%, with an average of 97.2%; the C_2H_6 content ranged from 0.28% to 0.99%, with an average of 0.48%; and the C_3H_8 content in all shale gas samples was very low, with an average of 0.01%. Non-hydrocarbon gases in the studied shale gas samples mainly consisted of N_2 (0.76%–3.11%, average: 1.39%) and CO_2 (0.01%–0.321%, average: 0.16%). The non-hydrocarbon gases He and Ar occurred in trace amounts in the shale gas samples and were detected using more precise noble gas mass spectrometry (the results are presented in Section 4.4).

4.3 Carbon and hydrogen isotope signatures of alkane gases

The $\delta^{13}C$ signatures of alkane gases varied among shale gas samples collected from different areas. The $\delta^{13}C_1$ values ranged from −36.5‰ to −29.6‰, with average values of −34.3‰, −33.8‰, −33.1‰, −30.7‰, and −30.8‰ for the PQ, DS, JF, WL, and PS areas, respectively. The $\delta^{13}C_2$ values ranged from −38.2‰ to −33.4‰, with average values of −37.1‰, −37.4‰, −36.2‰, −30.7‰, and −33.4‰ for the PQ, DS, JF, WL, and PS areas, respectively. The $\delta^{13}C$ signatures of alkane gases exhibited an increasing trend with

TABLE 2 Noble gas composition and isotopic data from normally pressured shale gas samples in the southeastern Sichuan Basin.

Area	Well	He (ppm)	Ne (ppm)	Ar (ppm)	$^{3}He/^{4}He$	err (1σ)	R/Ra	$^{20}Ne/^{22}Ne$	err(1σ)	$^{21}Ne/^{22}Ne$	err (1σ)	$^{4}He/^{20}Ne$	$^{40}Ar/^{36}Ar$	err (1σ)	$^{38}Ar/^{36}Ar$	err (1σ)
PQ	JY194-A	776.8	0.219	34	1.26E-08	1.20E-09	0.0091	10.8	0.11	0.028	0.0017	6,119.1	1,648.2	20	0.19	0.006
	JY194-B	573	0.028	—	1.80E-08	1.40E-09	0.0130	9.3	0.21	0.034	0.0039	36,263.4	—	—	—	—
	JY194-C	463.3	0.011	68	1.60E-08	1.90E-09	0.0116	10.7	0.37	0.035	0.0077	70,093.1	905.3	8.2	0.19	0.007
	JY195-A	449.6	0.029	38	1.40E-08	1.40E-09	0.0101	9.7	0.16	0.033	0.0027	33,320.6	1,011.6	7.4	0.19	0.003
	JY197-A	492.4	0.168	31	1.33E-08	1.80E-09	0.0096	10.8	0.13	0.032	0.0018	5,050.7	1,628.1	20	0.18	0.006
JF	JY204-A	396	0.118	29	1.44E-08	1.70E-09	0.0104	11.7	0.45	0.028	0.003	2,425.8	1,520	15	0.18	0.005
	JY204-B	491.4	0.012	31	8.06E-09	1.10E-09	0.0058	10.5	0.41	0.036	0.0066	69,002.8	1,561.2	18	0.19	0.005
	JY204-C	447.1	—	36	1.40E-08	1.80E-09	0.0101	11.5	0.17	0.03	0.0005		1,027.6	7.5	0.19	0.005
DS	SY-A	418	0.01	27	7.64E-09	1.10E-09	0.0055	10.7	0.51	0.034	0.0067	75,716.2	1,620.3	19	0.19	0.01
	SY-B	524.3	0.035	38	9.52E-09	1.80E-09	0.0069	10.6	0.16	0.036	0.0028	25,972.0	1,617.3	20	0.18	0.006
	SY-C	415.5	0.013	26	1.02E-08	1.30E-09	0.0074	11.2	0.42	0.035	0.0091	54,397.2	1,560.6	20	0.18	0.005
	SY-D	427.3	0.018	40	1.05E-08	1.40E-09	0.0076	11	0.24	0.037	0.0039	40,624.9	730.1	3.7	0.18	0.002
WL	LY-A	553	0.019	35	6.16E-09	1.00E-09	0.0045	10.9	0.23	0.039	0.0041	49,534.7	963.8	7	0.19	0.003
	LY-B	541.2	0.149	96	1.23E-08	1.70E-09	0.0089	11	0.14	0.031	0.0013	6,254.0	1,090.2	8.5	0.19	0.003
	PD-A	383.6	0.04	33	1.31E-08	1.60E-09	0.0095	11	0.2	0.031	0.0038	16,371.4	958.8	6.8	0.19	0.004
	LY-C	644.2	0.036	38	8.46E-09	1.60E-09	0.0061	9.6	0.16	0.032	0.0038	31,647.8	1,145.7	10	0.18	0.004
PS	PY-A	931.7	0.186	46	1.14E-08	3.00E-09	0.0082	10.5	0.13	0.03	0.0018	8,663.7	1,392.3	14	0.18	0.004
	PY-B	976.9	0.278	53	1.13E-08	1.70E-09	0.0082	10.4	0.13	0.03	0.0012	6,086.3	1,509.7	16	0.18	0.005

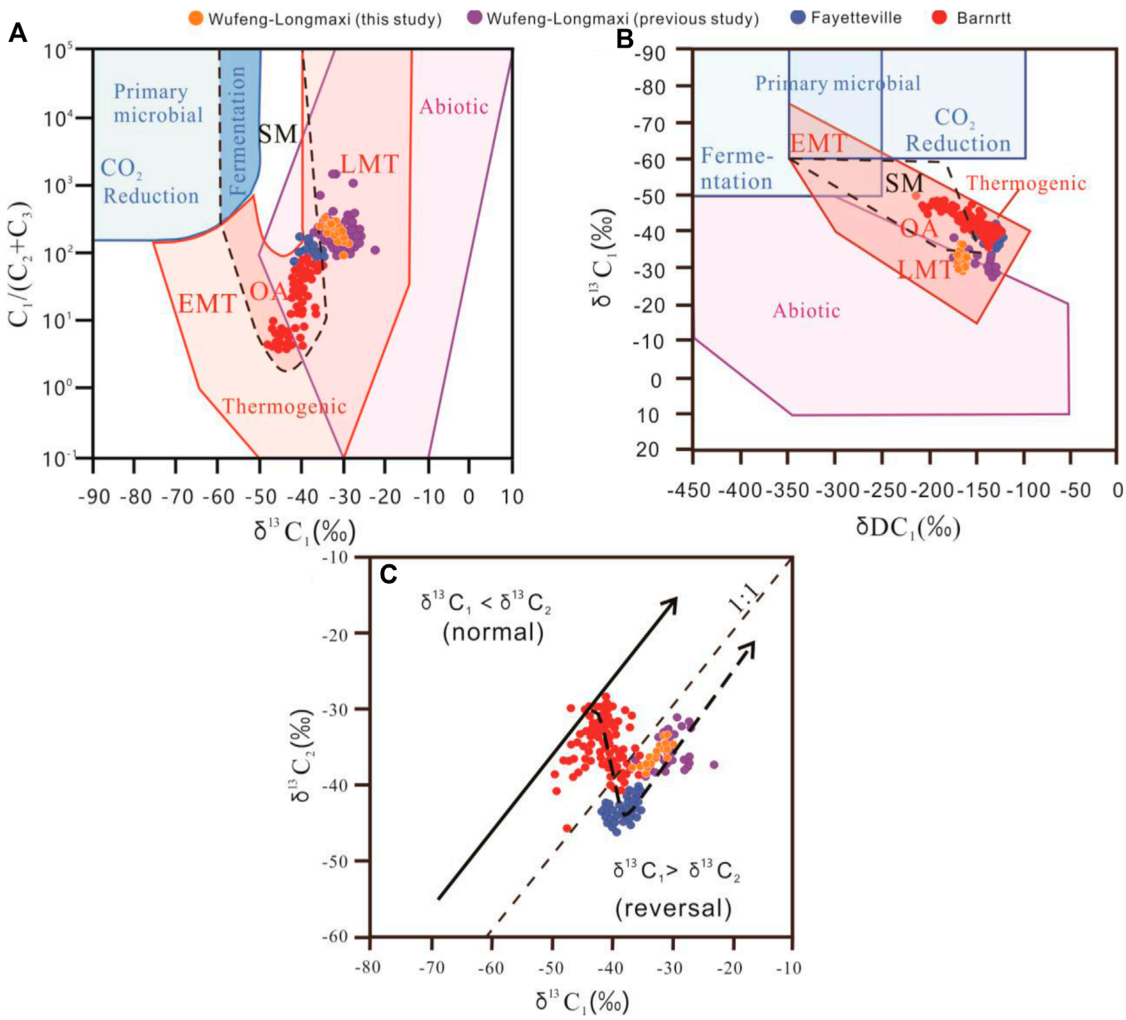

FIGURE 3
Gas molecular and stable isotope composition plots of normally pressured Longmaxi shale gas from the southeastern Sichuan Basin, along with other shales. **(A)** [$C_1/(C_2 + C_3)$] vs $\delta^{13}C_1$. **(B)** $\delta^{13}C_1$ vs δDC_1. **(C)** Isotopic composition of C_2H_6 exhibiting a reversal trend with increasing maturity. Fayetteville and Barnett shale gas data and genetic diagrams are adapted from Milkov et al. (2020), while previously studied shale gas data are adapted from Dai et al. (2014). Abbreviations: SM, secondary microbial; EMT, early-mature thermogenic gas; OA, oil-associated (mid-mature) thermogenic gas; LMT, late-mature thermogenic gas.

a decreasing pressure coefficient. In contrast to the $\delta^{13}C$ data, the δD signatures of alkane gases showed no evident pattern of change with a decreasing pressure coefficient, with δDC_1 ranging from −162.2‰ to −165.4‰ and δDC_2 ranging from −166.1‰ to −135.1‰.

4.4 Noble gas compositions and isotopes

He, Ne, and Ar concentrations and isotopic data from the 18 studied Longmaxi shale gas samples are presented in Table 2. The He concentration ranged from 383.6 to 976.9 ppm, with an average of 550.3 ppm. The He concentration varied among shale gas samples collected from different areas, showing an increasing trend with a decreasing pressure coefficient moving from the intra-basin toward the basin exterior. The average He contents of shale gas from the PQ, DS, JF, WL, and PS areas were 551.0, 446.2, 444.8, 530.5, and 954.3 ppm, respectively. Ne and Ar concentrations had ranges of 0.01–0.278 and 26–96 ppm, respectively.

$^3He/^4He$ ratios ranged from 0.0045 to 0.013 Ra, where Ra is the atmospheric ratio of (1.384 ± 0.013) × 10^{-6} (Ozima and Podosek, 2017; Mishima et al., 2018). $^{20}Ne/^{22}Ne$ ratios (9.3–11.7, average: 10.6) were higher than the atmospheric value (9.80; Sarda et al., 1988) and lower than the mantle value (12.2; Ballentine et al., 2005). $^4He/^{20}Ne$ ratios ranged from 2,425.8 to 75,716.2, much higher than the atmospheric value of 0.288 (Kipfer et al., 2002). Most $^{21}Ne/^{22}Ne$ ratios (0.028–0.039, average: 0.033) were higher than the atmospheric value (0.02959; Gyore et al., 2019), indicating a mixed source of two end-members: crustal (0.03–0.70; Ozima and Podosek, 2017) and atmospheric Ne. The $^{40}Ar/^{36}Ar$ ratios of the studied shale gas samples varied from 730.1 to 1,648.2, with an average of 1,286.7; these ratios are much higher than those of air, indicating no apparent noble gas contamination from the atmosphere during shale gas sampling and analysis.

5 Discussion

5.1 Coupling relationship between alkane gas isotopes and shale gas yield

The origin of Longmaxi shale gas has been widely discussed in previous studies (Hao et al., 2013; Dai et al., 2014; Wu et al., 2017; Cao et al., 2018; Liu et al., 2021). Methane is the dominant component in the high-/over-pressured Longmaxi shale gas produced (Dai et al., 2014; Liu et al., 2021). Normally pressured shale gas samples in the studied southeastern margin of the Sichuan Basin show similar characteristics, with high CH_4 abundance and high gas dryness ratios $[C_1/(C_2 + C_3)]$ (94.3–339.7, avg. 216.8). The δDC_1 values of normally pressured shale gas have a similar distribution range to those of Wufeng-Longmaxi shale gas from Weiyuan and Changning, as reported by Dai et al. (2014). Plots of $\delta^{13}C_1$ *versus* $[C_1/(C_2 + C_3)]$ (Figure 3A) and $\delta^{13}C_1$ *versus* δDC_1 (Figure 3B) both suggest that the Longmaxi shale gas is of late-mature thermogenic origin. A kinetic isotope effect resulting from differences in the energy required to cleave $^{12}C\backslash^{12}C$ and $^{12}C\backslash^{13}C$ bonds in shale gas precursors has been reported (Tang et al., 2000). Such a kinetic isotope effect results in a more positive $\delta^{13}C$ composition in hydrocarbons at higher maturity (Xia et al., 2013).

The $\delta^{13}C_1$ and $\delta^{13}C_2$ values of our normally pressured shale gas samples are plotted in Figure 3C, together with those of Barnett (Milkov et al., 2020), Fayetteville (Milkov et al., 2020), and Wufeng-Longmaxi (Dai et al., 2014) shale gas samples studied previously, in which the dashed line represents the relationship $\delta^{13}C_1 = \delta^{13}C_2$. Above the dashed line, a normal $\delta^{13}C$ trend exists, characterized by $\delta^{13}C_1 < \delta^{13}C_2$. The turning point in this normal trend area has been suggested to represent the start of secondary hydrocarbon cracking and mixing of gas (primary and secondary cracking), which would likely cause a $\delta^{13}C$ reversal among alkane gases (Tilley and Muehlenbachs, 2013; Xia et al., 2013). Shale gas with a normal $\delta^{13}C$ trend is mostly related to the low-middle stage of maturity. As maturity increases, a reversal in the trend ($\delta^{13}C_1 > \delta^{13}C_2$) can be observed. A further turning point in this reversed trend area has been suggested to represent a post-reversal stage at an extremely high or over-mature stage of evolution (Dai et al., 2014). This was confirmed by Xia et al. (2013) when applying a $\delta^{13}C$ correlated with the maturity model and by Wu et al. (2017) when studying even higher-maturity Lower Cambrian Niutitang shale gas.

For our normally pressured shale gas, $\delta^{13}C$ and δD data suggest that the shale gas originated from late-mature thermogenic generation, equivalent to shale gas in other production areas of the inner Sichuan Basin. The $[C_1/(C_2 + C_3)]$ data exhibit a negative relationship with $\delta^{13}C_1$ and $\delta^{13}C_2$ (Figure 4). Shale gas from the basin-margin transition belt (areas PQ, DS, and JF) is characterized by higher $[C_1/(C_2 + C_3)]$ and lighter $\delta^{13}C$ compared with shale gas samples from the extra-basin complex fold belt (areas WL and PS). The slope trend of decreasing $[C_1/(C_2 + C_3)]$ with heavier $\delta^{13}C$ matches the decreasing trend of the pressure coefficient for the selected shale gas samples. Meanwhile, daily shale gas yields for the selected production wells exhibit a negative correlation with $\delta^{13}C$ and a positive correlation with $[C_1/(C_2 + C_3)]$ (Figure 5), indicating that shale gas production wells in the basin-margin transition belt and extra-basin complex fold belt have completely different shale gas yields and gas geochemistry characteristics. The PS, DS, and JF areas have better gas production than WL and PS. The reason for this phenomenon may be that shale gas expulsion efficiency and gas source supply are different in different structural belts.

Meng et al. (2022) studied the CH_4 and C_2H_6 $\delta^{13}C$ changes in the Triassic Yanchang Formation from the Ordos Basin using pressure coring to avoid the problem of lost gas. During shale gas desorption, both $\delta^{13}C_1$ and $\delta^{13}C_2$ values became heavier, and gas dryness coefficients (C_1/C_{1-5}) decreased with increasing desorption rates. Smaller molecules (e.g., CH_4) desorb more rapidly than longer-chain hydrocarbon gases. For normally pressured shale gas, variations in gas geochemistry characteristics provide evidence for the gas accumulation and expulsion processes during geological time. The WL and PS areas within the extra-basin complex fold belt experienced earlier uplift compared with the PQ, DS, and JF areas within the basin-margin transition belt (Figure 6, modified after Teng et al., 2020). Although shale layers in the WL and PS areas have similar top and bottom cap-rock conditions to those in the inner basin area (e.g., Fulin shale gas field), their relatively poor self-sealing capacity and low displacement pressure mean that an episodic hydrocarbon expulsion process is more likely to occur. More oil and gas escape from these shale layers during the peak hydrocarbon generation period, reducing the potential source supply for later shale gas generation during higher maturity stages. During expulsion, hydrocarbons with a lighter $\delta^{13}C$ escape first, leaving the residual hydrocarbons richer in ^{13}C. As the pressure coefficient decreases, the hydrocarbon expulsion efficiency increases and residual gas abundance is reduced. Therefore, the PS shale gas samples are characterized by the heaviest $\delta^{13}C$ values, lowest gas dryness coefficients, and lowest daily gas yields among all studied shale gas samples.

The H atom is much smaller than the C atom; hence, H isotope fractionation occurs more readily during shale gas expulsion or desorption. Notably, unlike $\delta^{13}C$, the δD values of CH_4 and C_2H_6 show little variation with changes in pressure coefficient across all studied shale gas samples. A previous study suggested that δD values in alkane gases desorbed from pressure coring remained stable with increasing gas desorption rates (Meng et al., 2022).

5.2 Origin of noble gases in a normally pressured shale gas system

In subsurface fluid systems, noble gases can have atmospheric, mantle, or radiogenic origins, with distinct isotopic signatures associated with each component (Ballentine et al., 2005). According to its origin, there are three types of He: atmospheric, mantle-derived, and crust-derived. Helium has two isotopes: primordial ^3He and ^4He sourced from the radioactive decay of ^{238}U, ^{235}U, and ^{232}Th over geological time (Graham, 2002). The origin of He is usually determined using the ratio of the isotopic abundances of ^3He and ^4He, i.e., $R = {}^3He/{}^4He$. Atmospheric He is ubiquitous in the air, showing no industrial significance, owing to its low concentration. The R value for atmospheric helium is 1.4×10^6, normally referred to as Ra. Mantle-derived He refers to He of deep magmatic origin, including the original ^3He captured in the early

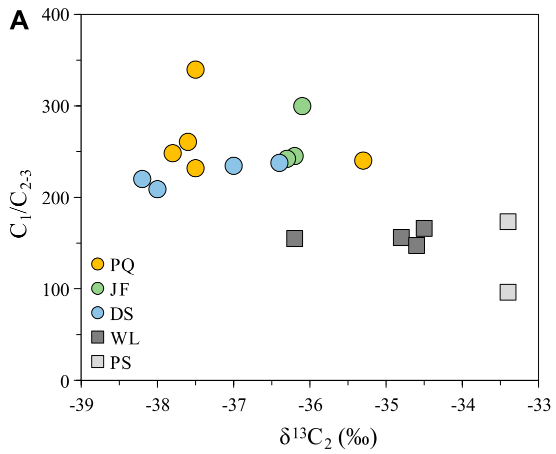

FIGURE 4
Correlations between the dryness coefficient (C_1/C_{2-3}) and $\delta^{13}C$. **(A)** C_1/C_{2-3} vs $\delta^{13}C_1$. **(B)** C_1/C_{2-3} vs $\delta^{13}C_2$.

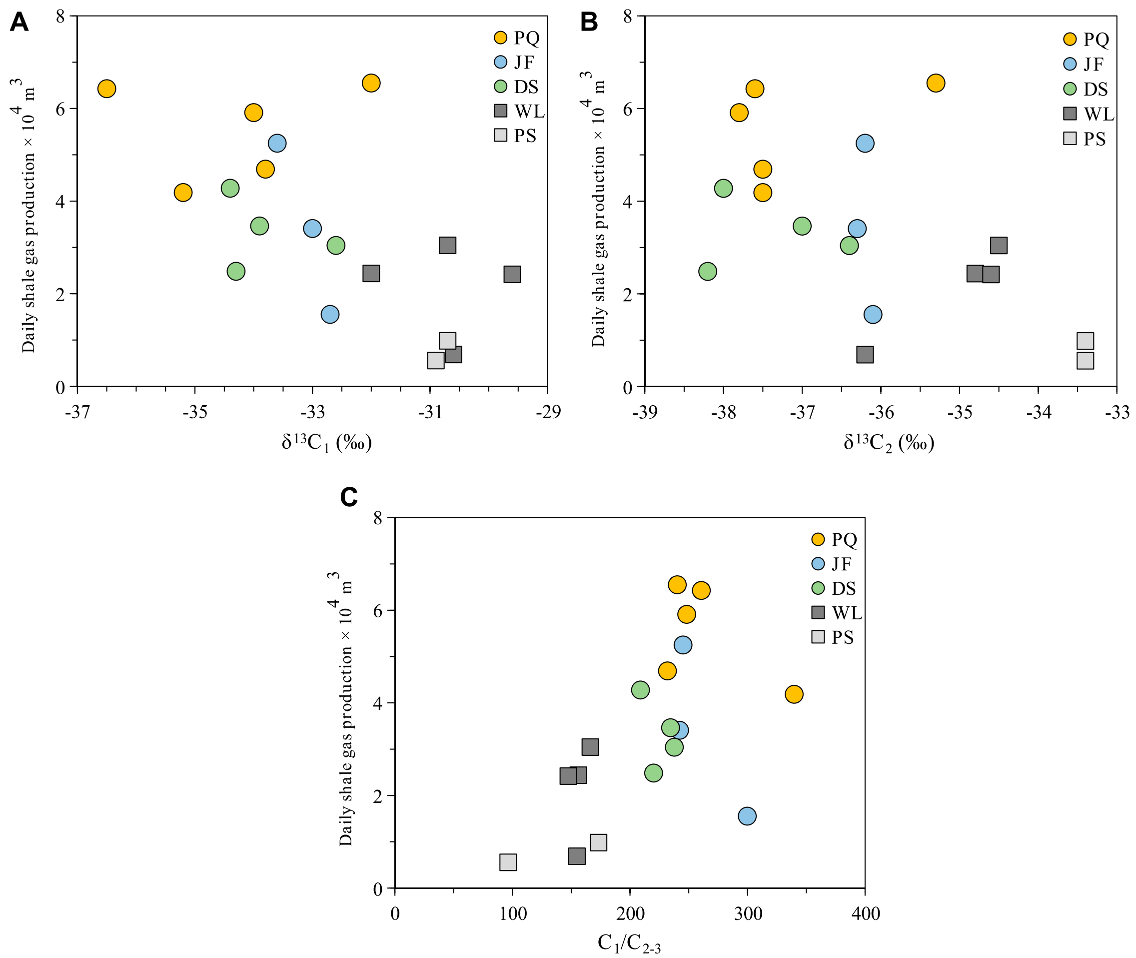

FIGURE 5
Correlations between daily shale gas production and hydrocarbon gas geochemistry characteristics. Daily shale gas production vs $\delta^{13}C_1$ **(A)**, $\delta^{13}C_2$ **(B)**, and dryness coefficient (C_1/C_{2-3}) **(C)**.

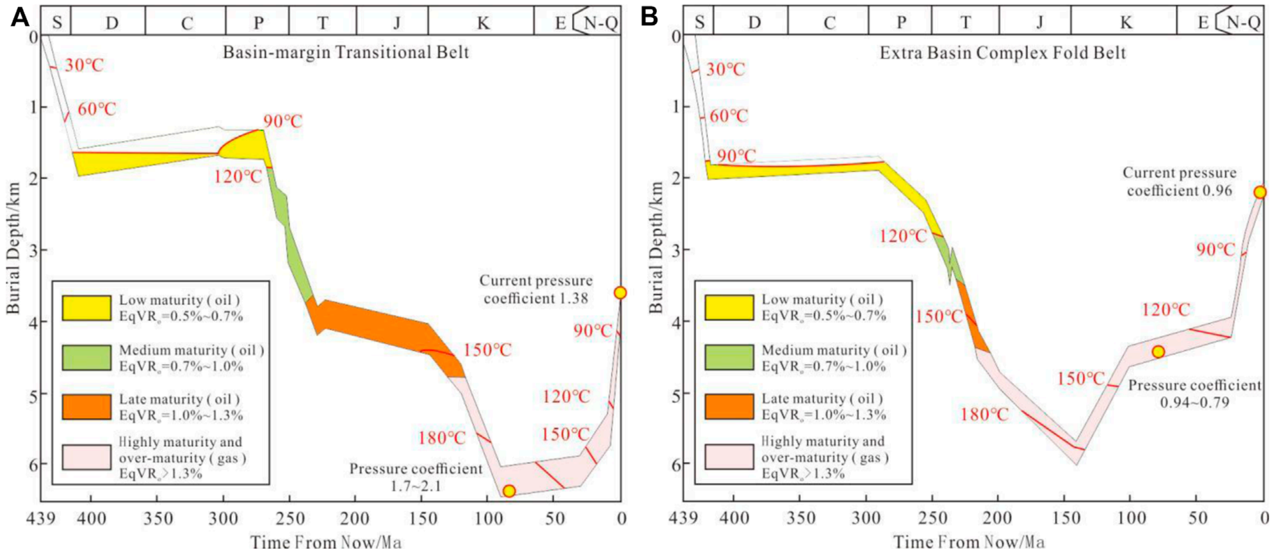

FIGURE 6
Burial history, thermal history, and paleo-pressure of the Wufeng-Longmaxi Formation in the **(A)** basin-margin transition belt and **(B)** extra-basin complex fold belt.

stage of the formation of the Earth, and ^{4}He produced by radioactive decay, with a high R ratio of approximately 8 Ra. Crust-derived He is mainly sourced from α radioactive decay of U and Th in ancient sedimentary rocks, metamorphic rocks, migmatites, and granites. This crust-derived He, with a low R ratio of approximately 0.02 Ra, is an important source of He input in natural gas reservoirs (Oxburgh et al., 1986; Ballentine and Lollar, 2002; Kennedy and van Soest, 2005; Wang et al., 2020). As shown in a plot of R/Ra vs ^{4}He/^{20}Ne (Figure 7A), the ^{3}He/^{4}He ratios (R/Ra) of our normally pressured shale gas samples range from 0.0045 to 0.013 Ra, all plotted within the crust end-member region. A plot of CH_4/^{3}He vs R/Ra (Figure 7B) also indicates that the studied shale gas samples lie in the crustal field, suggesting that the Longmaxi shale gas received a substantial contribution of crust-derived He; this is consistent with the Weiyuan and Changning shale gas samples studied by Cao et al. (2020).

Argon has three isotopes, namely, ^{40}Ar, ^{38}Ar, and ^{36}Ar, with ^{40}Ar mainly sourced from the radioactive decay of K, and ^{38}Ar and ^{36}Ar of primordial origin (Ballentine and Burnard, 2002). The ^{40}Ar/^{36}Ar ratios of our shale gas samples are relatively high (Figure 8; ranging from 1,194.3 to 4,604.5), indicating a radiogenic origin consistent with that suggested by the He isotope data. The ^{40}Ar/^{36}Ar ratios of our shale gas samples exhibit similar values to those of Jiaoshiba shale gas but are higher than those of Changning shale gas samples from the southern Sichuan Basin (Wang et al., 2022).

5.3 Shale gas accumulation and expulsion reflected in noble gas isotope signatures

Compared with conventional natural gas reservoirs, the enrichment and preservation of noble gas and the controlling factors of the formation of He-rich natural gas reservoirs show some similarities and also differences. Regions with high hydrocarbon generation intensity that are conducive to the formation of large oil and gas reservoirs may not be conducive to the formation of He-rich natural gas reservoirs. However, tectonic uplift and denudation areas with relatively low hydrocarbon generation intensity may be favorable for forming He-rich natural gas. The same applies to shale gas reservoirs, in which self-generation and self-storage occur. Excessive hydrocarbon generation intensity greatly dilutes the concentration of He. Therefore, for self-generated and self-stored He-rich shale gas reservoirs, despite the high content of U and Th in shale, it is difficult to achieve commercial development of He, owing to the dilution effect of hydrocarbon gases (Wang et al., 2020). The He concentration of Wufeng-Longmaxi shale gas is relatively low in the high-yield Jiaoshiba and Changning areas, with average concentrations of 205 and 376 ppm, respectively. However, in extra-basin areas that are structurally complex, the He concentration can reach 941 ppm (Wang et al., 2022).

The spatial distributions of He and Ar concentrations have been suggested to be closely related to the accumulation and dissipation of shale gas (Wang et al., 2022). Owing to mixing and dilution, the concentration of He decreases with an increase in the shale gas content. Compared with shale gas development areas in a structurally stable basin, such as Changning and Jiaoshiba, the preservation conditions of shale gas in structurally complex areas outside the basin, such as Pengshui in southeastern Chongqing, are relatively poor. At the over-mature evolution stage, owing to the continuous decay of U and Th releasing ^{4}He, higher He contents are found in structurally complex areas outside the basin compared with inner basin areas with high shale gas production.

As shown in Figure 9, the He and Ar concentrations of shale gas samples from the basin-margin transition belt (PQ, DS, and JF areas) are lower than those of the extra-basin complex fold belt (WL and PS areas). The He and Ar concentrations of PS shale gas samples in this study are consistent with previous data (He: 716–941 ppm, Ar: 42–56 ppm; Wang et al., 2022). The contents of ^{4}He and ^{40}Ar show

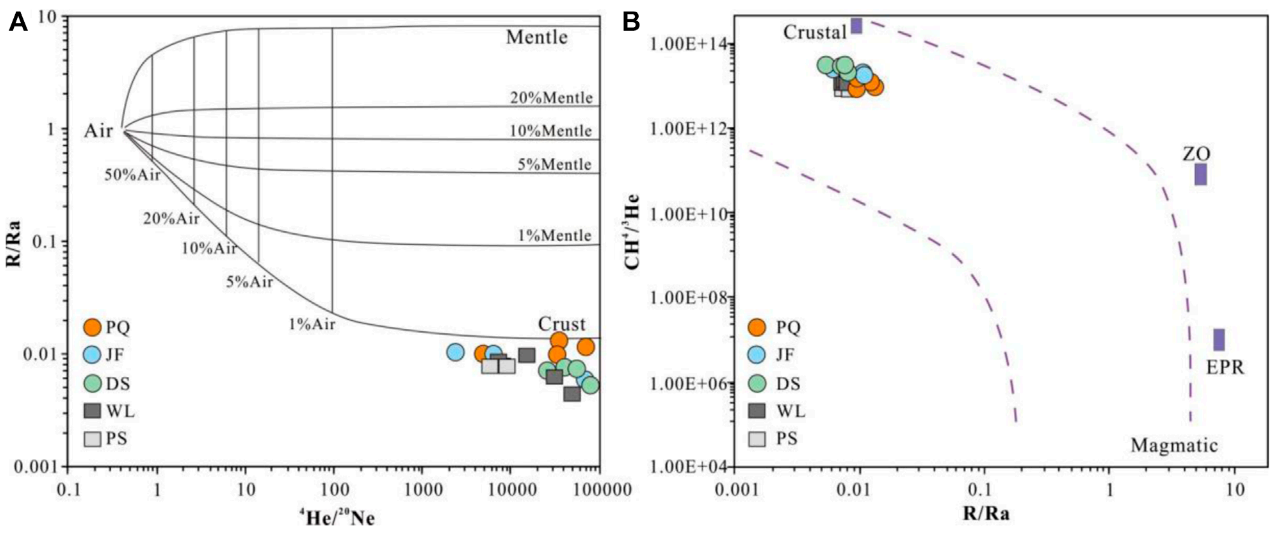

FIGURE 7
(A) Plot of $^{3}He/^{4}He$ (R/Ra) vs $^{4}He/^{20}Ne$ showing mixing lines between the atmosphere and upper mantle and between the atmosphere and crust. Ratios of the atmosphere, continental crust, and upper mantle end-members are obtained from Ozima and Podosek (2017), Ballentine and Burnard (2002), and Graham (2002). **(B)** Plot of $CH_4/^{3}He$ vs $^{3}He/^{4}He$ (R/Ra) demonstrating a crustal origin for noble gases.

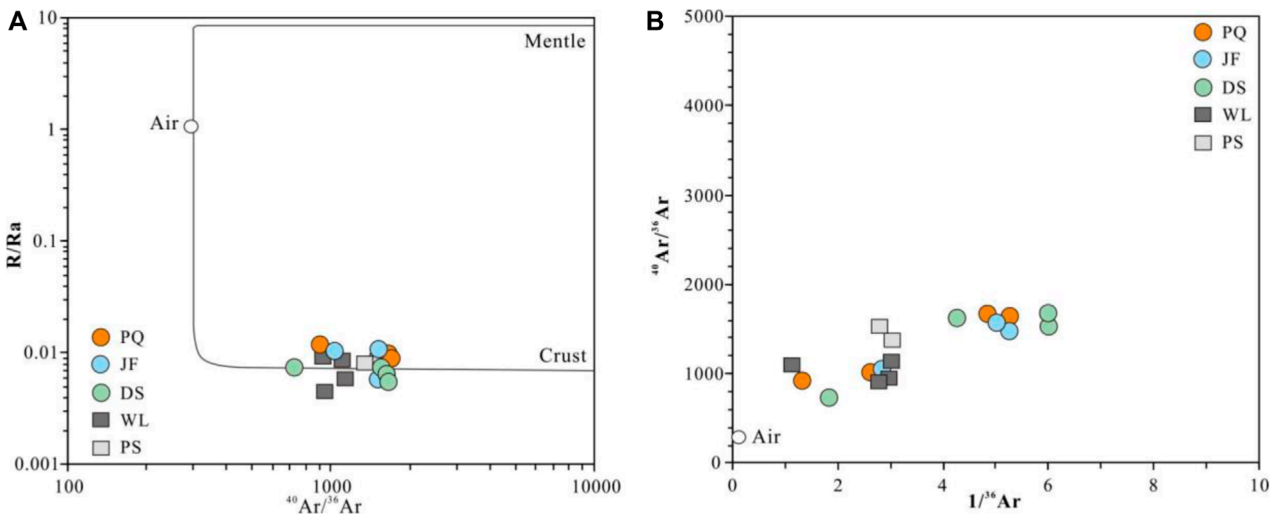

FIGURE 8
Plots of **(A)** $^{3}He/^{4}He$ (R/Ra) vs $^{40}Ar/^{36}Ar$ and **(B)** $^{40}Ar/^{36}Ar$ vs $1/^{36}Ar$.

a weak positive correlation (Figure 10A), indicating a radiogenic contribution for both noble gases.

The He content exhibits a negative correlation with daily shale gas yield for the studied shale gas wells (Figure 10B). High-gas yield wells located in structural regions with higher *in situ* stress and higher pressure coefficients have low concentrations of He and Ar. As an unconventional gas, shale gas has the characteristics of self-generation and self-storage. A large amount of gas can be generated during the hydrocarbon gas generation stage. However, the abundance of noble gas (He and Ar) source elements, such as U, Th, and K, is very low in geological bodies, with an extremely long half-life and a very low rate of He or Ar generation ($1\ m^3$ km−3 year−^{1}). Furthermore, there is no peak of concentrated noble gas generation during the generation and storage processes. After the termination of the hydrocarbon generation process, the concentrations of He and Ar will inevitably be diluted with increasing CH_4 concentrations (Li et al., 2022).

The correlations between He and $\delta^{13}C$ are shown in Figure 11. The ^{4}He content exhibits positive correlations with both $\delta^{13}C_1$ and $\delta^{13}C_2$, with WL and PS shale gas samples having the highest ^{4}He contents and heaviest $\delta^{13}C$ signatures. The PQ and DS shale gas samples have the lowest ^{4}He contents and the lightest $\delta^{13}C$ signatures, with JF shale gas samples having intermediate values.

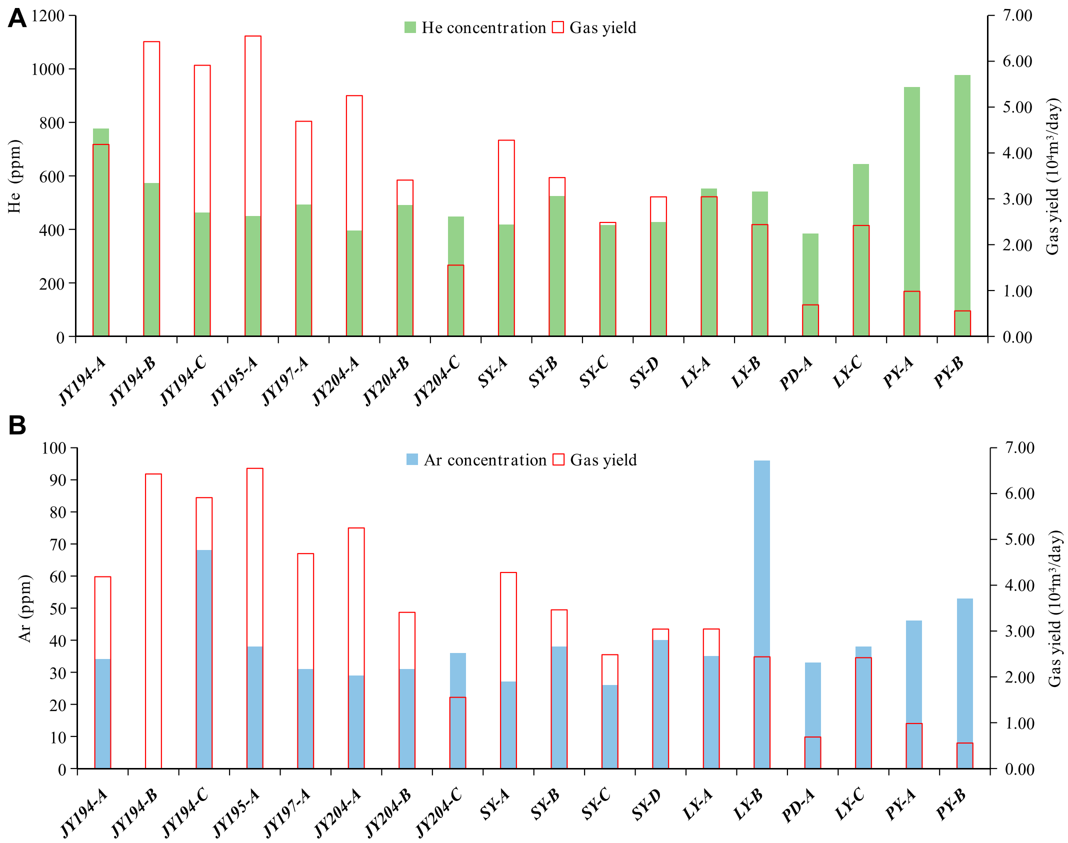

FIGURE 9
Noble gas abundances and gas yield distribution for the normally pressured shale gas studied. **(A)** He abundance. **(B)** Ar abundance.

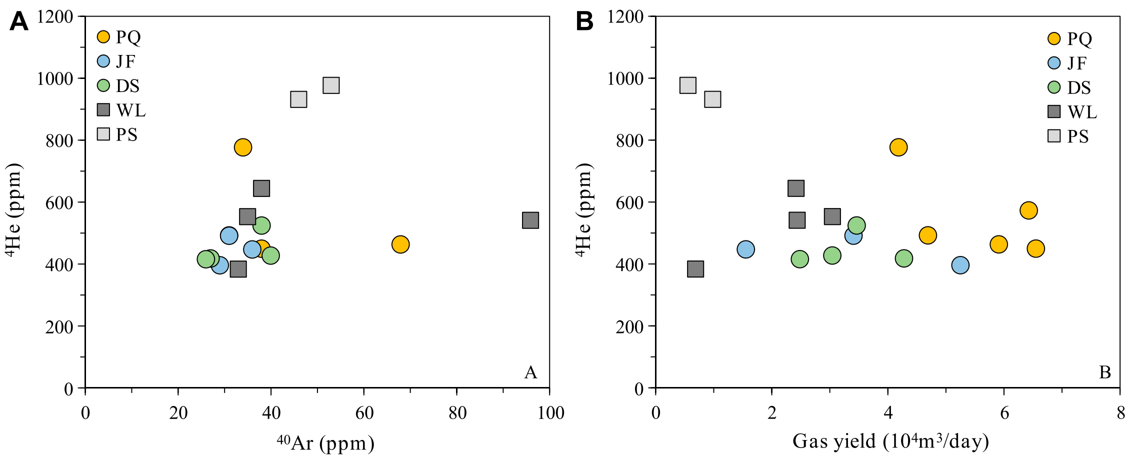

FIGURE 10
Plots of **(A)** ^{4}He vs ^{40}Ar content and **(B)** ^{4}He vs gas yield.

The above coupled noble gas and stable isotope analyses reveal that the concentrations of He and Ar and δ^{13}C signatures of alkane gases are closely related to the accumulation and expulsion of shale gas. Generally, with an increasing pressure coefficient, shale gas preservation conditions become better, and high shale gas yields are attained, which will dilute the concentration of noble gases. Furthermore, better preservation conditions equate to less shale gas escaping during the gas generation period, causing δ^{13}C values to remain closer to their initial values. In contrast, shale gas preserved under poor conditions loses lighter hydrocarbons and

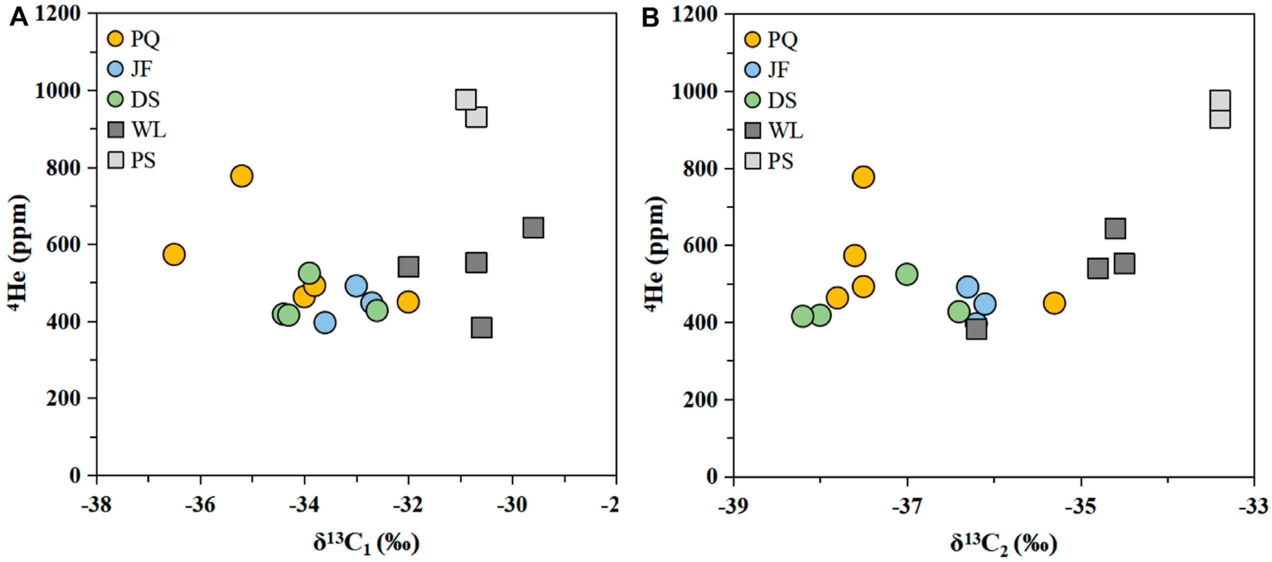

FIGURE 11
Correlations between ^{4}He abundance and δ^{13}C. **(A)** ^{4}He vs $\delta^{13}C_1$. **(B)** ^{4}He vs $\delta^{13}C_2$.

isotopes, causing decreasing pressure coefficients and residual gases rich in heavy components. For shale gas reservoirs characterized by a wide range of pressure coefficients, such as the normally pressured Marcellus (pressure coefficient between 0.9 and 1.4; Chalmers et al., 2012) and highly pressured Haynesville (pressure coefficient between 1.61 and 2.07; Hammes et al., 2011) shale gas fields in North America, shale gas production exhibits a similar positive correlation with an increasing pressure coefficient to that found herein. Therefore, gas geochemical data may also provide effective indicators for shale gas production evaluation in these regions. Compared with tectonically stable regions, which exhibit fewer differences in gas geochemical characteristics, the noble gas and stable isotope distribution trends presented herein for tectonically active regions will be more effective in evaluating shale gas accumulation and expulsion in shale gas reservoirs worldwide.

6 Conclusion

On the basis of our systematic study of the noble gas and stable isotope characteristics of normally pressured shale gas samples, which are part of a continuous pressure coefficient series from the southeastern Sichuan Basin, our preliminary conclusions are as follows:

(1) Stable δ^{13}C and δD data revealed that the shale gas originated from late-mature thermogenic generation, similar to shale gas from other production areas within the inner Sichuan Basin. As the pressure coefficient decreased, the hydrocarbon expulsion efficiency increased and residual gas abundance decreased. Shale gas from the basin-margin transition belt (PQ, DS, and JF areas) was characterized by a higher dryness ratio and a lighter δ^{13}C signature than shale gas from the extra-basin complex fold belt (WL and PS areas).

(2) Noble gas isotopes were used to reveal the origin of noble gas in the normally pressured shale gas system studied. The ^{3}He/^{4}He ratios (R/Ra) ranged from 0.0045 to 0.013 Ra, and the ^{40}Ar/^{36}Ar ratios were relatively high, suggesting that the shale gas was sourced from a typically radiogenic origin.

(3) High-gas-yield wells located in structural areas with higher *in situ* stress and higher pressure coefficients had low concentrations of He and Ar. The He content showed positive correlations with $\delta^{13}C_1$ and $\delta^{13}C_2$ values. Shale gas samples from the WL and PS areas were characterized by the highest He contents and heaviest δ^{13}C signatures. Our coupled noble gas and δ^{13}C and δD data revealed that the concentrations of He and Ar and δ^{13}C signatures of alkane gases are closely related to the accumulation and expulsion of shale gas.

(4) In tectonically stable regions, shale gas reservoirs normally exhibit favorable conditions with only relatively small differences in gas geochemistry. In tectonically active regions, shale gas geochemical characteristics exhibit substantial differences related to changes in structure. Better preservation conditions accompanied by lower-intensity tectonic movement normally result in higher shale gas production and a lower concentration of noble gases. The above results indicate that gas geochemical characteristics can be used as effective evaluation indicators for determining shale gas accumulation mechanisms in structurally active regions.

Data availability statement

The original contributions presented in the study are included in the article/Supplementary Material; further inquiries can be directed to the corresponding author.

Author contributions

JL: writing–original draft and writing–review and editing. YW: writing–original draft and writing–review and editing. DF: project administration and writing–review and editing. ZW: writing–review and editing. CW: writing–original draft.

Funding

The author(s) declare that financial support was received for the research, authorship, and/or publication of this article. This work was conducted as part of a project funded by Sinopec East China Oil and Gas Company with grant no. 34600355-23-FW2099-0051.

Acknowledgments

The authors are grateful to Sinopec East China Oil and Gas Company for access to samples and associated data. They are sincerely grateful to the Chief Editor, Valerio Acocella, and the reviewers who provided valuable comments.

Conflict of interest

Authors JL, YW, and DF were employed by Sinopec East China Oil and Gas Company.

The remaining authors declare that the research was conducted in the absence of any commercial or financial relationships that could be construed as a potential conflict of interest.

Publisher's note

All claims expressed in this article are solely those of the authors and do not necessarily represent those of their affiliated organizations, or those of the publisher, the editors, and the reviewers. Any product that may be evaluated in this article, or claim that may be made by its manufacturer, is not guaranteed or endorsed by the publisher.

References

Ballentine, C. J., and Burnard, P. G. (2002). Production, release and transport of noble gases in the continental crust. *Rev. Mineral. Geochem.* 47, 481–538. doi:10.2138/rmg.2002.47.12

Ballentine, C. J., and Lollar, B. S. (2002). Regional groundwater focusing of nitrogen and noble gases into the Hugoton-Panhandle giant gas field, USA. *Geochem. Cosmochim. Acta* 66, 2483–2497. doi:10.1016/S0016-7037(02)00850-5

Ballentine, C. J., Marty, B., and Sherwood, L. B. (2005). Neon isotopes constrain convection and volatile origin in the Earth's mantle. *Nature* 433, 33–38. doi:10.1038/nature03182

Burnard, P., Zimmermann, L., and Sano, Y. (2013). "The noble gases as geochemical tracers: history and background," in *The noble gases as geochemical tracers. Advances in isotope geochemistry*. Editor P. Burnard (Berlin, Heidelberg: Springer), 1–15. doi:10.1007/978-3-642-28836-4_1

Byrne, D. J., Barry, P. H., Lawson, M., and Ballentine, C. (2018). Determining gas expulsion vs retention during hydrocarbon generation in the Eagle Ford Shale using noble gases. *Geochim. Cosmochim. Acta* 241, 240–254. doi:10.1016/j.gca.2018.08.042

Byrne, D. J., Barry, P. H., Lawson, M., and Ballentine, C. (2020). The use of noble gas isotopes to constrain subsurface fluid flow and hydrocarbon migration in the East Texas Basin. *Geochim. Cosmochim. Acta* 268, 186–208. doi:10.1016/j.gca.2019.10.001

Byrne, D. J., Barry, P. H., Lawson, M., and Ballentine, C. J. (2017). Noble gases in conventional and unconventional petroleum systems. *Geol. Soc. Lond., Spec. Publ.* 468, 127–149. doi:10.1144/sp468.5

Cao, C., Zhang, M., Li, L., Wang, Y., Li, Z., Du, L., et al. (2020). Tracing the sources and evolution processes of shale gas by coupling stable (C, H) and noble gas isotopic compositions: cases from Weiyuan and Changning in Sichuan Basin, China. *J. Nat. Gas. Sci. Eng.* 78, 103304. doi:10.1016/j.jngse.2020.103304

Cao, C., Zhang, M., Tang, Q., Yang, Y., Lv, Z., Zhang, T., et al. (2018). Noble gas isotopic variations and geological implication of Longmaxi shale gas in Sichuan Basin, China. *China. Mar. Petrol. Geol.* 89, 38–46. doi:10.1016/j.marpetgeo.2017.01.022

Chalmers, G., Bustin, R., and Power, I. (2012). Characterization of gas shale pore systems by porosimetry, pycnometry, surface area, and field emission scanning electron microscopy/transmission electron microscopy image analyses: examples from the Barnett, Woodford, Haynesville, Marcellus, and Doig units. *Aapg Bull.* 96, 1099–1119. doi:10.1306/10171111052

Chen, Z., Chen, L., Wang, G., Zou, C., Jiang, S., Si, Z., et al. (2020). Applying isotopic geochemical proxy for gas content prediction of Longmaxi shale in the Sichuan Basin, China. *China. Mar. Petrol. Geol.* 116, 104329. doi:10.1016/j.marpetgeo.2020.104329

Curtis, J. B. (2002). Fractured shale-gas systems. *AAPG Bull.* 86, 1921–1938. doi:10.1306/61EEDDBE-173E-11D7-8645000102C1865D

Dai, J., Zou, C., Liao, S., Dong, D., Ni, Y., and Huang, J. (2014). Geochemistry of the extremely high thermal maturity Longmaxi shale gas, southern Sichuan Basin. *Org. Geochem.* 74, 3–12. doi:10.1016/j.orggeochem.2014.01.018

Darabi, H., Ettehad, A., Javadpour, F., and Sepehrnoori, K. (2012). Gas flow in ultra-tight shale strata. *J. Fluid. Mech.* 710, 641–658. doi:10.1017/jfm.2012.424

Dong, D., Zou, C., Dai, J. X., Huang, S., Zheng, J., Gong, J., et al. (2016). Suggestions on the development strategy of shale gas in China. *J. Nat. Gas. Geosci.* 1, 413–423. doi:10.1016/j.jnggs.2016.11.011

Gao, L., Schimmelmann, A., Tang, Y., and Mastalerz, M. (2014). Isotope rollover in shale gas observed in laboratory pyrolysis experiments: insight to the role of water in thermogenesis of mature gas. *Org. Geochem.* 68, 95–106. doi:10.1016/j.orggeochem.2014.01.010

Graham, D. W. (2002). Noble gas isotope geochemistry of mid-ocean ridge and ocean island basalts: characterization of mantle source reservoirs. *Rev. Mineral. Geochem.* 47, 247–317. doi:10.2138/rmg.2002.47.8

Guo, C., Xu, J., Wu, K., Wei, M., and Liu, S. (2015). Study on gas flow through nano pores of shale gas reservoirs. *Fuel* 143, 107–117. doi:10.1016/j.fuel.2014.11.032

Guo, T. (2016). Key geological issues and main controls on accumulation and enrichment of Chinese shale gas. *Petrol. explor. Dev.* 43, 349–359. doi:10.1016/S1876-3804(16)30042-8

Guo, T., Jiang, S., and Zhang, P. (2020). Progress and direction of exploration and development of normally-pressured shale gas from the periphery of Sichuan Basin. *J. Petroleum Geol. Exp.* 42, 837–845. doi:10.11781/sysydz202005837

Győre, D., Tait, A., Hamilton, D., and Stuart, F. M. (2019). The formation of NeH^+ in static vacuum mass spectrometers and re-determination of $^{21}Ne/^{20}Ne$ of air. *Geochim. Cosmochim. Acta* 263, 1–12. doi:10.1016/j.gca.2019.07.059

Hammes, U., Hamlin, H., and Ewing, T. (2011). Geologic analysis of the upper jurassic Haynesville shale in east Texas and west Louisiana. *J. Biol. Chem.* 95, 1643–1666. doi:10.1306/02141110128

Hao, F., Zou, H., and Lu, Y. (2013). Mechanisms of shale gas storage: implications for shale gas exploration in China. *AAPG Bull.* 97, 1325–1346. doi:10.1306/02141312091

He, X. (2021). Sweet spot evaluation system and enrichment and high yield influential factors of shale gas in Nanchuan area of eastern Sichuan Basin. *Nat. Gas. Ind.* 41, 59–71. doi:10.3787/j.issn.1000-0976.2021.01.005

He, X., Qi, Y., and He, G. (2019). Further understanding of main controlling factors of normal pressure shale gas enrichment and high yield in the area with complex structure of the southeast area of Chongqing. *Reserv. Eval. Dev.* 5, 32–39. doi:10.13809/j.cnki.cn32-1825/te.2019.05.004

Hu, Q., Liu, X., Gao, Z., Liu, S. G., Zhou, W., and Hu, W. X. (2015). Pore structure and tracer migration behavior of typical American and Chinese shales. *Petrol. Sci.* 12, 651–663. doi:10.1007/s12182-015-0051-8

Jiang, S., Li, C., and Chen, G. (2022). Occurrence of normally-pressured shale gas in China and the United States and their effects on mobility and production: a case study of southeast Sichuan Basin and Appalachia Basin. *Petroleum Reserv. Eval. Dev.* 12, 399–406. doi:10.13809/j.cnki.cn32-1825/te.2022.03.001

Jiang, Z., Song, Y., Tang, X., Li, Z., Wang, X., Wang, G., et al. (2020). Controlling factors of marine shale gas differential enrichment in southern China. *Petrol. explor. Dev.* 47, 661–673. doi:10.1016/S1876-3804(20)60083-0

Kennedy, B. M., and van Soest, M. C. (2005). A helium isotope perspective on the Dixie Valley, Nevada, hydrothermal system. *Geothermics* 35, 26–43. doi:10.1016/j.geothermics.2005.09.004

Kipfer, R., Aeschbach-Gertig, W., Peeteres, F., and Stute, M. (2002). Noble gases in lakes and ground waters. *Rev. Mineral. Geochem.* 47, 615–700. doi:10.2138/rmg.2002.47.14

Lancaster, D. E., Guldry, F. K., Graham, R. L., Curtis, J., Shaw, J., and Blake, T. (1989). A case study of the evaluations completion and testing of a Devonian shale gas well. *J. Petrol. Technol.* 41, 509–518. doi:10.2118/17037-PA

Li, Y., Li, J., and Zhou, J. (2022). Research progress and new views of evaluation of helium resources. *J. Sci. Environ.* 44, 363–373. doi:10.19814/j.jese.2021.11008

Liu, R., Wen, T., Julien, A., Zheng, J., Hao, F., and Jiang, D. (2021). The dichotomy in noble gas signatures linked to tectonic deformation in Wufeng-Longmaxi Shale, Sichuan Basin. *Chem. Geol.* 581, 120412. doi:10.1016/j.chemgeo.2021.120412

Ma, X., Li, X., Liang, F., Wan, Y., Shi, Q., Wang, Y., et al. (2020). Dominating factors on well productivity and development strategies optimization in Weiyuan shale gas play, Sichuan Basin, SW China. *Petrol. explor. Dev.* 47, 594–602. doi:10.1016/S1876-3804(20)60076-3

Meng, M., Zhang, Y., Yuan, B., and Li, Z. (2023). Imbibition behavior of oil-saturated rock: implications for enhanced oil recovery in unconventional reservoirs. *Energy and Fuels* 37 (18), 13759–13768. doi:10.1021/acs.energyfuels.3c02501

Meng, Q., Wang, X., Shi, B., Lei, Y., Zhao, H., Zhao, Q., et al. (2022). The ^{13}C-depleted methane in terrigenous shale gas: a case study in the Triassic Yanchang Formation, Ordos Basin. *Mar. Petrol. Geol.* 141, 105688. doi:10.1016/j.marpetgeo.2022.105688

Milkov, A. V., Faiz, M., and Etiope, G. (2020). Geochemistry of shale gases from around the world: composition, origins, isotope reversals and rollovers, and implications for the exploration of shale plays. *Org. Geochem.* 143, 103997. doi:10.1016/j.orggeochem.2020.103997

Mishima, K., Sumino, H., Yamada, T., Ieki, S., Nagakura, N., Otono, H., et al. (2018). Accurate determination of the absolute ^{3}He/^{4}He ratio of a synthesized helium standard gas (helium standard of Japan, HESJ): toward revision of the atmospheric ^{3}He/^{4}He ratio. *Geochem. Geophys. Geosyst.* 19, 3995–4005. doi:10.1029/2018GC007554

Montgomery, S. L., Jarvie, D. M., Bowker, K. A., and Pollastro, R. M. (2006). Mississippian Barnett Shale, Fort Worth basin, north-central Texas: gas-shale play with multi–trillion cubic foot potential. *AAPG Bull.* 89, 155–175. doi:10.1306/09170404042

Oxburgh, E. R., O'Nions, R. K., and Hill, R. I. (1986). Helium isotopes in sedimentary basins. *Nature* 324, 632–635. doi:10.1038/324632a0

Ozima, M., and Podosek, F. A. (2017). *Noble gas geochemistry*. 2nd edition. New York: Cambridge University Press. doi:10.1017/cbo9780511545986

Pollastro, R. M., Jarvie, D. M., Hill, R. J., and Adams, C. W. (2007). Geologic framework of the mississippian Barnett shale, barnett-paleozoic total petroleum system, bend arch–fort worth basin, Texas. *AAPG Bull.* 91, 405–436. doi:10.1306/10300606008

Qiu, Z., Zou, C., and Wang, H. (2020). Discussion on the characteristics and controlling factors of differential enrichment of Wufeng-Longmaxi formations shale gas in south China. *Nat. Gas. Geosci.* 31, 163–175. doi:10.1016/j.jnggs.2020.05.004

Sarda, P., Staudacher, T., and Allegre, C. J. (1988). Neon isotopes in submarine basalts. *Earth Planet. Sci. Lett.* 91, 73–88. doi:10.1016/0012-821X(88)90152-5

Schoell, M. (1988). Multiple origins of methane in the Earth. *Chem. Geol.* 71 (1), 1–10. doi:10.1016/0009-2541(88)90101-5

Tang, Y., Perry, J. K., Jenden, P. D., and Schoell, M. (2000). Mathematical modeling of stable carbon isotope ratios in natural gases. *Geochimica Cosmochimica Acta* 64, 2673–2687. doi:10.1016/s0016-7037(00)00377-x

Teng, G., Tao, C., and Hu, G. (2020). Effect of hydrocarbon expulsion efficiency on shale gas formation and enrichment. *Pet. Geol. Exp.* 42, 325–334. doi:10.11781/sysydz202003325

Tilley, B., and Muehlenbachs, K. (2013). Isotope reversals and universal stages and trends of gas maturation in sealed, self-contained petroleum systems. *Chem. Geol.* 339, 194–204. doi:10.1016/j.chemgeo.2012.08.002

Wang, P., Shen, Z., Liu, S., Lv, Z., Zhu, T., and Gong, Y. (2013). Geochemical characteristics of noble gases in natural gas and their application in tracing natural gas migration in the middle part of the western Sichuan Depression, China. *Petrol. Sci.* 10, 327–335. doi:10.1007/s12182-013-0281-6

Wang, X., Liu, W., Li, X., Liu, Q., Tao, C., and Xu, Y. (2020). Radiogenic helium concentration and isotope variations in crustal gas pools from Sichuan Basin, China. *Appl. Geochem.* 117, 104586. doi:10.1016/j.apgeochem.2020.104586

Wang, X., Liu, W., Li, X., Tao, C., Borjigin, T., Liu, P., et al. (2022). Application of noble gas geochemistry to the quantitative study of the accumulation and expulsion of lower Paleozoic shale gas in southern China. *Appl. Geochem.* 146, 105446. doi:10.1016/j.apgeochem.2022.105446

Whiticar, M. J. (1996). Stable isotope geochemistry of coals, humic kerogens and related natural gases. *Int. J. Coal Geol.* 32, 191–215. doi:10.1016/S0166-5162(96)00042-0

Wu, C. J., Tuo, J. C., Zhang, L. F., Zhang, M., Li, J., Liu, Y., et al. (2017). Pore characteristics differences between clay-rich and clay-poor shales of the Lower Cambrian Niutitang Formation in the Northern Guizhou area, and insights into shale gas storage mechanisms. *Int. J. Coal Geol.* 178, 13–25. doi:10.1016/j.coal.2017.04.009

Xia, X., Chen, J., Braun, R., and Tang, Y. (2013). Isotopic reversals with respect to maturity trends due to mixing of primary and secondary products in source rocks. *Chem. Geol.* 339, 205–212. doi:10.1016/j.chemgeo.2012.07.025

Xia, X. Y., and Tang, Y. C. (2012). Isotope fractionation of methane during natural gas flow with coupled diffusion and adsorption/desorption. *Geochem. Cosmochim. Acta* 77, 489–503. doi:10.1016/j.gca.2011.10.014

Xing, L., Li, Z., Li, L., and Liu, Y. (2021). Application of chromium catalysis technology to compound-specific hydrogen isotope analysis of natural gas samples. *Talanta* 239, 123133. doi:10.1016/j.talanta.2021.123133

Zhang, W., Li, Y., Zhao, F., Han, W., Zhou, J., Holland, G., et al. (2019). Quantifying the helium and hydrocarbon accumulation processes using noble gases in the North Qaidam Basin, China. *Chem. Geol.* 523, 368–379. doi:10.1016/j.chemgeo.2019.07.020

Zhao, W., Jia, A., and Wei, Y. (2020). Progress in shale gas exploration in China and prospects for future development. *China Pet. Explor.* 25, 31–44. doi:10.3969/j.issn.1672-7703.2020.01.004

Zhao, W., Zhang, S., He, K., Zeng, H., Hu, G., Zhang, B., et al. (2019). Origin of conventional and shale gas in Sinian–lower Paleozoic strata in the Sichuan Basin: relayed gas generation from liquid hydrocarbon cracking. *AAPG Bull.* 103, 1265–1296. doi:10.1306/11151817334

Zhou, Z., Ballentine, C. J., Schoell, M., and Stevens, S. H. (2012). Identifying and quantifying natural CO_2 sequestration processes over geological timescales: the Jackson Dome CO_2 Deposit, USA. *Geochim. Cosmochim. Acta* 86, 257–275. doi:10.1016/j.gca.2012.02.028

Zou, C., Yang, Z., Dai, J., Dong, D., Zhang, B., Wang, Y., et al. (2015). The characteristics and significance of conventional and unconventional Sinian–Silurian gas systems in the Sichuan Basin, central China. *Mar. Petrol. Geol.* 64, 386–402. doi:10.1016/j.marpetgeo.2015.03.005

Zou, C., Zhao, Q., and Wang, H. (2021). Theory and technology of unconventional oil and gas exploration and development helps China increase oil and gas reserves and production. *Petroleum Sci. Technol. Forum.* 40, 72–79. doi:10.3969/j.issn.1002-302x.2021.03.007